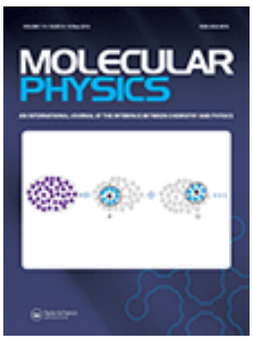

Molecular Physics

An International Journal at the Interface Between Chemistry and Physics

ISSN: 0026-8976 (Print) 1362-3028 (Online) Journal homepage: http://www.tandfonline.com/loi/tmph20

The time-dependent density matrix renormalisation group method

Haibo Ma, Zhen Luo & Yao Yao

To cite this article: Haibo Ma, Zhen Luo & Yao Yao (2017): The time-dependent density matrix renormalisation group method, Molecular Physics, DOI: 10.1080/00268976.2017.1406165

To link to this article: https://doi.org/10.1080/00268976.2017.1406165

Published online: 30 Nov 2017.

MOLECULAR PHYSICS, 2017
https://doi.org/10.1080/00268976.2017.1406165

Taylor & Francis
Taylor & Francis Group

MOLECULAR PHYSICS IN CHINA

The time-dependent density matrix renormalisation group method

Haibo Ma[a], Zhen Luo[a] and Yao Yao[b]

[a]School of Chemistry and Chemical Engineering, Nanjing University, Nanjing, China; [b]Department of Physics, South China University of Technology, Guangzhou, China

ABSTRACT

Substantial progress of the time-dependent density matrix renormalisation group (t-DMRG) method in the recent 15 years is reviewed in this paper. By integrating the time evolution with the sweep procedures in density matrix renormalisation group (DMRG), t-DMRG provides an efficient tool for real-time simulations of the quantum dynamics for one-dimensional (1D) or quasi-1D strongly correlated systems with a large number of degrees of freedom. In the illustrative applications, the t-DMRG approach is applied to investigate the nonadiabatic processes in realistic chemical systems, including exciton dissociation and triplet fission in polymers and molecular aggregates as well as intersystem crossing in pyrazine molecule.

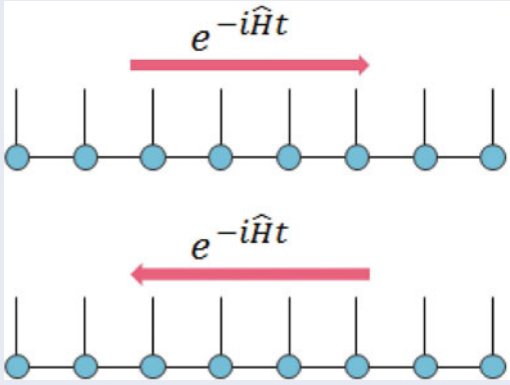

ARTICLE HISTORY
Received 28 September 2017
Accepted 31 October 2017

KEYWORDS
Density matrix renormalisation group; matrix product state; time-dependent density matrix renormalisation group; nonadiabatic dynamics; quantum dynamics

1. Introduction

The density matrix renormalisation group (DMRG) method, invented by White in 1992 [1], has nowadays been considered as a well-established numerical method of studying one-dimensional (1D) strongly correlated quantum systems. DMRG uses the eigenvalues of the subsystem's reduced density matrix as the decimation criterion of the Hilbert space and keeps a fixed number (M) of renormalised states during the enlargement of the system, and thus it can be efficiently applied to very large 1D systems. Low-energy equilibrium properties of both bosonic and fermionic 1D and quasi-1D many-body systems can be calculated at almost machine precision and comparatively low computational cost by virtue of using DMRG. Recent efforts have advanced DMRG successfully working in some two-dimensional (2D) systems. For example, the ground state of 2D spin-1/2 Kagome lattice was evidenced to be fully gapped [2], and the composite fermions on a 2D electron gas under a strong magnetic field are determined to be massless Dirac particles [3] by DMRG calculations. In the recent two decades, the applicability of DMRG has gone successfully beyond theoretical condensed matter physics, and was extended to a wide range of fields ranging from statistical mechanics [4] to quantum chemistry [5–11] as well as quantum information theory [12,13]. The readers can find extensive reviews on DMRG in Refs. [14–17].

Following the success of DMRG for finding the true equilibrium or steady-state quantities, many time-dependent variants of DMRG (t-DMRG) [18–36] have also been developed in the recent 15 years to explore the real-time quantum dynamics of 1D strongly correlated systems. These developments provide useful tools to understand how the quantum many-body systems response to the external time-dependent perturbations

CONTACT Haibo Ma haibo@nju.edu.cn; Yao Yao yaoyao2016@scut.edu.cn

and to calculate their dynamics far from equilibrium. The t-DMRG method was firstly introduced by Cazalilla and Marston [18] in 2002 and then later improved by Luo, et al. [19] and Schmitteckert [21] as well as Feiguin and White [22], Dutta and Ramasesha [24] to exploit the real-time dynamics in quantum many-body systems out of equilibrium. They used a static t-DMRG scheme, in which the truncated Hilbert space for approximating $|\Psi(t=0)\rangle$ is gradually enlarged with the evolving time to ensure a large overlap with the exact result of $|\Psi(t)\rangle$. Obviously, the deviation of $|\Psi(t)\rangle$ from $|\Psi(t=0)\rangle$ increasing with the evolving time, and accordingly more and more states are necessary to be kept in the truncated Hilbert space as time evolves. Therefore, the static t-DMRG scheme suffers from a great limitation that the computational costs would be very expensive or prohibitive for long-time simulations.

In order to simulate the quantum dynamics of 1D strongly correlated systems more efficiently, in 2004 White and Feiguin [25] and Daley et al. [26] proposed t-DMRG using adaptive Hilbert spaces (later termed as the adaptive t-DMRG), in which one fixes the size of the truncated Hilbert space, but tries to change it as time evolves so that this adapted space can describe $|\Psi(t)\rangle$ to a very good approximation. Such adaptive t-DMRG methods are mainly based on the time-evolving block decimation (TEBD) algorithm [37,38], and the key ingredient of TEBD-based methods is a Suzuki-Trotter [39,40] splitting of the Hamiltonian to the individual terms $\hat{H} = \sum_i \hat{h}_i$. When these terms are local, the propagation operator $e^{i\hat{H}\Delta t}$ can be applied efficiently to the DMRG wavefunction. Such an adaptive t-DMRG method has been successfully applied to the studies of spin-charge separation in cold Fermi gases [41], dynamical quasicondensation of hard-core Bosons at finite momenta [42], and far-from-equilibrium properties of interacting nanostructures [43], as well as many others [44–56].

Unfortunately, the TEBD idea is not applicable to Hamiltonians with long-range interactions, which appear in quasi-2D systems or quantum chemistry applications as well as system-bath problems. For system-bath problems, in 2008 one of the authors (H.M.) [27] and the other one (Y.Y.) [28] and their colleagues independently combined the adaptive t-DMRG with Ehrenfest dynamics to implement real-time quantum simulations for an electron-phonon model at the mean field level. Later in 2010, Prior et al. [29] combined an exact analytical mapping of the problem onto an effective 1D system and the adaptive t-DMRG to implement real-time simulation for strong system-bath interactions at the full quantum dynamics level. This has been successfully applied to study the ultrafast electronic processes in organic condensed phase with a large number of vibrational modes [57,58].

Recent advances of the theory about matrix product state (MPS) [59–61] and matrix product operator (MPO) [62,63] have also been incorporated into t-DMRG for more efficient propagation of a quantum state by Haegeman et al. [31,32] and Zaletel et al. [33]. They have shown that, the MPS representation of the t-DMRG wavefunction based on time-dependent variational principle (TDVP) [64,65] or an approximation of the evolution operator in terms of MPO, can greatly simplify the procedures for the time propagation of the many-body wavefunction and does not rely on the form of the Hamiltonians, expanding the toolbox of studying general quantum dynamics for systems beyond 1D topologies and Hamiltonians containing long-range interactions.

In this short overview, we will briefly review the developments of t-DMRG in the last 15 years since its invention by Cazalilla and Marstonin in 2002 [18]. We will first introduce the basic ideas in MPS and DMRG, and then discuss the detailed schemes of t-DMRG and its many variants as well as its recent applications on electron-phonon systems. Finally, we will give a brief summary and outlook.

2. Matrix product state (MPS) and density matrix renormalisation group (DMRG)

Here, we give a brief introduction to MPS and DMRG. For their details, we refer the readers to the excellent reviews [14–17].

2.1. MPS

Let us first assume a 1D quantum lattice of L sites, in which each site i=1, 2, … , L has a d-dimensional local state space $\{\sigma_i\}$. A most general description for a quantum state on this lattice is

$$|\psi\rangle = \sum_{\sigma_1,\ldots,\sigma_L} c_{\sigma_1,\sigma_2,\ldots,\sigma_L} |\sigma_1\rangle \otimes |\sigma_2\rangle \otimes \ldots \otimes |\sigma_L\rangle, \quad (1)$$

where the number of full configurations $|\sigma_1\rangle\otimes|\sigma_2\rangle \otimes\ldots\otimes|\sigma_L\rangle$ and their coefficients $c_{\sigma_1,\sigma_2,\ldots,\sigma_L}$ is d^L, exponentially increasing with the system size L.

If we reshape the state vector $c_{\sigma_1,\sigma_2,\ldots,\sigma_L}$ with the dimension d^L into a matrix Ψ of dimension $d \times d^{L-1}$ ($\Psi_{\sigma_1,(\sigma_2,\ldots,\sigma_L)} = c_{\sigma_1,\sigma_2,\ldots,\sigma_L}$), a singular value decomposition (SVD) can lead to

$$\Psi_{\sigma_1,(\sigma_2,\ldots,\sigma_L)} = \sum_{a_1} U_{\sigma_1,a_1} S_{a_1} V^{\dagger}_{a_1,(\sigma_2,\ldots,\sigma_L)}, \quad (2)$$

where the U-matrix has dimension $d \times d$. At the next step, we can define a new matrix $\Psi_{(a_1\sigma_2),(\sigma_3,\ldots,\sigma_L)} = S_{a_1} V^{\dagger}_{a_1,(\sigma_2,\ldots,\sigma_L)}$ with a dimension $(d^2 \times d^{L-2})$, where the row dimension may be smaller if singular values of the previous SVD happen to be zero. This can be decomposed again with an SVD as follows:

$$\Psi_{(a_1\sigma_2),(\sigma_3,\ldots,\sigma_L)} = \sum_{a_2} U_{(a_1,\sigma_2),a_2} S_{a_2} V^{\dagger}_{a_2,(\sigma_3,\ldots,\sigma_L)}, \quad (3)$$

with the dimension of the U-matrix being $d^2 \times d^2$. Through successive SVD decompositions, one can obtain

$$|\psi\rangle = \sum_{\sigma_1\ldots,\sigma_L} \sum_{a_1,\ldots,a_{L-1}} U_{\sigma_1,a_1} U_{(a_1\sigma_2),a_2} \ldots U_{(a_{L-1}\sigma_L),1} |\sigma_1\rangle \otimes |\sigma_2\rangle \otimes \ldots \otimes |\sigma_L\rangle. \quad (4)$$

In order to simplify the notation, one can define d matrices A^{σ_i} for each site by $A^{\sigma_i}_{a_{i-1},a_i} = U_{(a_{i-1},\sigma_i),a_i}$, and then the quantum state reads

$$|\psi\rangle = \sum_{\sigma_1\ldots\sigma_L} A^{\sigma_1} A^{\sigma_2} \ldots A^{\sigma_L} |\sigma_1\rangle \otimes |\sigma_2\rangle \otimes \ldots \otimes |\sigma_L\rangle. \quad (5)$$

One should note that the dimensions of $A^{\sigma_1}, \ldots, A^{\sigma_L}$ are $1 \times d$, $d \times d^2, \ldots, d^{L/2-1} \times d^{L/2}$, $d^{L/2} \times d^{L/2-1}, \ldots, d^2 \times d$ and $d \times 1$, respectively. For many systems of interests, $d^{L/2}$ will be too huge and accordingly the exact MPS representation will be intractable for $L \geq 16$ (d=4) or $L \geq 32$ (d=2). Under such circumstances, efficient approximations for A^{σ_i} matrices become necessary.

2.2. DMRG

To overcome the difficulty in MPS representation for large L, one can impose constraints on the dimensions of A^{σ_i} matrices to be no larger than a fixed number of M (usually from 10^1 to 10^4, far less than $d^{L/2}$). Now the main task of the determination of an MPS wave function is to optimise $d \times L$ A^{σ_i} matrices. But this is still computationally infeasible because optimising $d \times L$ matrices simultaneously is a non-linear problem. However, it can be reduced to a linear problem by the DMRG sweep algorithm [1], by which the variational parameters in the MPS wave function can be variationally determined by just iteratively optimising one or two of the matrices A^i while keeping all other matrices fixed. Usually the M is fixed by a specific number, or dynamically adjusted in a dynamical block state selection (DBSS) protocol [66].

Below we will briefly show how to iteratively optimise A^{σ_i} matrices. The key notion in the MPS-DMRG framework is that of local updates [62]. Instead of modifying an A^{σ_i} matrix directly, one can introduce an additional matrix C into the MPS:

$$A^{\sigma_1} A^{\sigma_2} \ldots A^{\sigma_n} C A^{\sigma_{n+1}} \ldots A^{\sigma_L}. \quad (6)$$

We directly modify only the matrix C which simplifies the local optimisation problem as C is just an ordinary matrix. To introduce the local degrees of freedom, say for the $|\sigma_n\rangle$ states, we expand the basis for A^{σ_n}. That is, the $M \times M$-dimensional matrices A^{σ_n} are replaced by the $M \times dM$-dimensional matrices $A^{'\sigma_n}$

$$A^{'\sigma_n}_{ij} = \delta_{i \times d + \sigma_n, j}, \quad (7)$$

and we introduce the $dM \times M$-dimensional matrix

$$C_{i \times d + \sigma_n, k} = A^{\sigma_n}_{ik}. \quad (8)$$

Such a transformation does not change any physics of the quantum state, as $A^{'\sigma_n} C = A^{\sigma_n}$. Similarly, one can expand the basis for the $A^{\sigma_{n+1}}$ matrix on the right side of C simultaneously, in order to optimise two A^{σ_i} matrix at once.

Using the centre matrix C in Equation (8) as an input to an eigensolver for the ground state of the Hamiltonian, one can get the new optimised C matrix at site n. The optimisation for A^{σ_n} can be accomplished by $A^{\sigma_n} = A^{'\sigma_n} U$, in which the $dM \times M$-dimensional matrix U can be obtained from an SVD ($C = UDV\dagger$). It should be noted that U and V matrices can be also calculated as the eigenvectors of the reduced density matrices (RDMs) $\rho_L = CC\dagger$ and $\rho_R = C\dagger C$ for the left ($|\sigma_1\rangle \otimes \ldots \otimes |\sigma_n\rangle$) and right ($|\sigma_{n+1}\rangle \otimes \ldots \otimes |\sigma_L\rangle$) subsystems, and this is why such a method is termed as DMRG.

We can repeat the above operations for sites $n+1$, $n+2, \ldots$, until $L-1$ to optimise $A^{\sigma_{n+1}}$, $A^{\sigma_{n+2}}, \ldots$, and $A^{\sigma_{L-1}}$ successively. After the end of this right half-sweep (growth of the left subsystem and shrinkage of the right subsystem), one can reverse the optimisation direction by starting the left half-sweep (shrinkage of the left subsystem and growth of the right subsystem), as shown in Figure 1.

The operations in left sweep is similar to those in right sweep, but the main difference is that the introduction of the the centre matrix C in Equation (6) is used for the update of $A^{\sigma_{n+1}}$ instead of A^{σ_n}. In such cases, we expand the basis for the $A^{\sigma_{n+1}}$ matrix on the right side of C, i.e. the $dM \times M$-dimensional matrices $A^{'\sigma_{n+1}}$

$$A^{'\sigma_{n+1}}_{ij} = \delta_{i, j \times d + \sigma_{n+1}}, \quad (9)$$

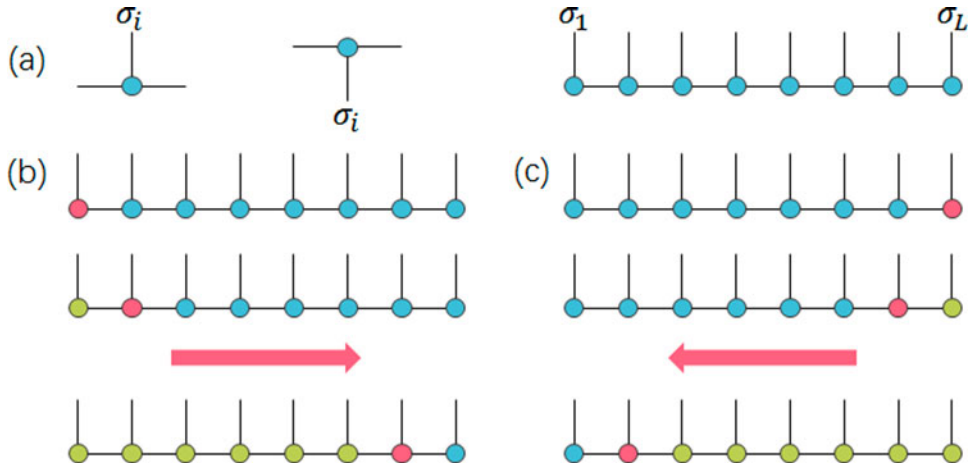

Figure 1. (a) Graphical representation of a matrix product state (MPS) constituent, a matrix $A^{\sigma_n}_{ab'}$ its conjugate, and of an MPS. Note that on the first and last sites, the matrices reduce to row and column vectors (one horizontal leg only). The evaluation rule is to contract over all connected legs. (b) Graphic representation of the left half-sweep DMRG iterations. (c) Graphic representation of the right half-sweep DMRG iterations. The red circle denotes the active site.

and the $M \times dM$-dimensional matrix

$$C_{k,j\times d+\sigma_{n+1}} = A^{\sigma_{n+1}}_{kj} \tag{10}$$

are introduced. With the optimised C through the eigen-solution for the ground state of the Hamiltonian, one can optimise $A^{\sigma_{n+1}}$ by $A^{\sigma_{n+1}} = V^{\dagger}A'^{\sigma_{n+1}}$, where the $dM \times M$-dimensional matrix V can be obtained from an SVD ($C = UDV\dagger$) or the eigen-solution for $\rho_R = C\dagger C$. Similarly, one can repeat the above operations for sites $n, n-1, \ldots,$ until 2 to optimise A^{σ_n}, $A^{\sigma_{n-1}}, \ldots,$ and A^{σ_2} successively. After the end of this left half-sweep, one can reverse the optimisation direction again by starting the right half-sweep, as shown in Figure 1. Usually, a complete shrinkage and growth sequence for both subsystems is called a sweep, including a left half-sweep and a right half-sweep.

The sweeping through the system is continued until energy (or, more precisely, the wave function) converges. The intuitive motivation for this (in practice highly successful) procedure is that after several sweeps, all A^{σ_i} matrices in Equation (5) have been optimised in the presence of an ever improved embedding and finally they arrived at self-consistency.

3. Static time-dependent density matrix renormalisation group

In 2002, Cazalilla and Marston (CM) [18] firstly proposed to evolve the quantum state by integrating the time-dependent Schrödinger equation within the truncated Hilbert space after a standard DMRG calculation to the Hamiltonian $\hat{H}(t=0)$. In their static t-DMRG framework, the initial state is chosen to be the ground state of the unperturbed truncated Hamiltonian ($\hat{H}_{\text{trunc}}$), i.e. $|\Psi(t=0)\rangle = |\Psi^{\text{DMRG}}_{\text{GS}}\rangle$. Then a time-dependent perturbation, $\hat{H}'(t)$, is added to $\hat{H}_{\text{trunc}}$, and the time-dependent Schrödinger equation is integrated forward in time:

$$i\hbar\frac{\partial}{\partial t}|\Psi(t)\rangle = [(\hat{H}_{\text{trunc}} - E_0) + \hat{H}'(t)]|\Psi(t)\rangle, \tag{11}$$

where E_0 is the ground state energy of $\hat{H}_{\text{trunc}}$. Forward integration can be numerically carried out by step-size adaptive methods such as fourth-order Runge–Kutta (RK4) integration based on the infinitesimal time-evolution operator. In RK4 algorithm, the new state at time $t + \Delta t$ can be calculated by:

$$|\Psi(t+\Delta t)\rangle \simeq \frac{1}{6}[|\chi_1\rangle + 2|\chi_2\rangle + 2|\chi_3\rangle + |\chi_4\rangle] + O(\Delta t^5), \tag{12}$$

where the four intermediate vectors are:

$$\begin{aligned}
|\chi_1\rangle &= \Delta t(\hat{H}(t) - E_0)|\Psi(t)\rangle,\\
|\chi_2\rangle &= \Delta t(\hat{H}(t+\Delta t/2) - E_0)\left[|\Psi(t)\rangle + \frac{1}{2}|\chi_1\rangle\right],\\
|\chi_3\rangle &= \Delta t(\hat{H}(t+\Delta t/2) - E_0)\left[|\Psi(t)\rangle + \frac{1}{2}|\chi_2\rangle\right],\\
|\chi_4\rangle &= \Delta t(\hat{H}(t+\Delta t) - E_0)[|\Psi(t)\rangle + |\chi_3\rangle].
\end{aligned} \tag{13}$$

As an alternative to integrating the time-dependent Schrödinger equation numerically, Schmitteckert [21] proposed the direct application of the time-evolution operator $U(\Delta t)=\exp(-i\hat{H}(t)\Delta t/\hbar)$ to obtain the new quantum state $|\Psi(t+\Delta t)\rangle = U(\Delta t)|\Psi(t)\rangle$. Although the exact determination of $\exp(-i\hat{H}(t)\Delta t/\hbar)$ is infeasible for

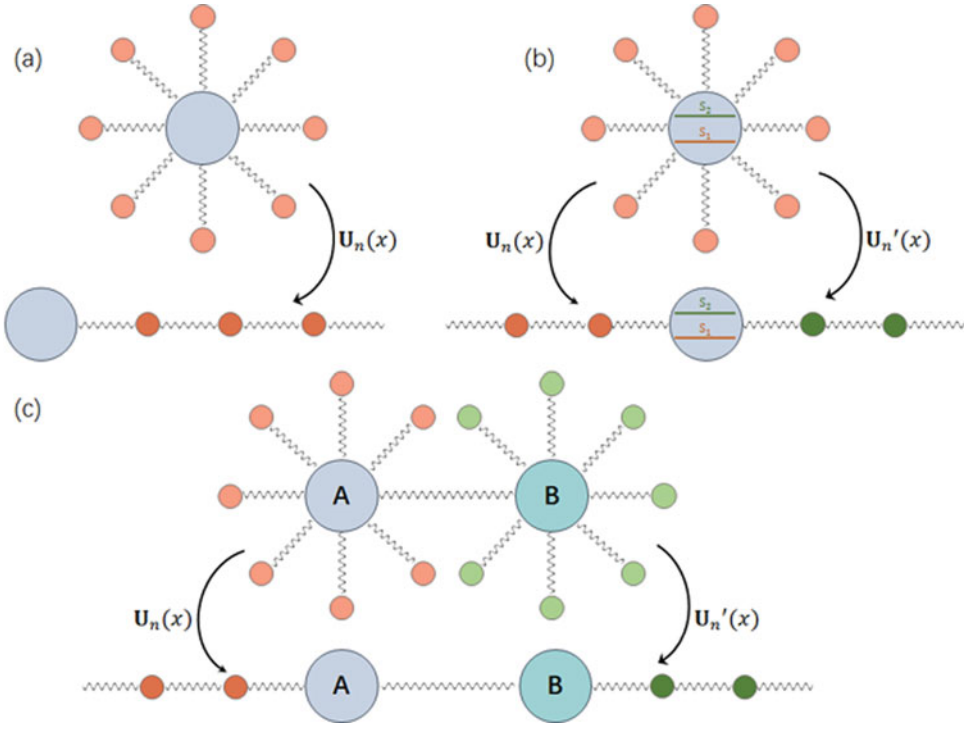

Figure 2. Unitary transformations for various standard system-bath Hamiltonians to 1D chain-like Hamiltonians with only nearest neighbor interactions. For example, (a) the standard spin-Boson Hamiltonian where the two spin states have the same couplings with the phonon bath; (b) chemical systems where the two electronic states have different couplings with the phonon bath; and (c) the dimer model which have two different baths.

large matrix dimensions, one can calculate the action of a matrix exponential on a state vector very similar to Lanczos sparse matrix diagonalisation [67]. In detail, one can use standard DMRG to calculate the m lowest eigenstates $|\Phi_i\rangle$ for $\hat{H}(t)$, i.e. $\hat{H}(t)|\Phi_j\rangle = E_j|\Phi_j\rangle$, and represent the new state at time $t + \Delta t$ by

$$\hat{P} = \sum_{j=0}^{m-1} |\Phi_j\rangle\langle\Phi_j|, \tag{14}$$

$$|\Psi(t+\Delta t)\rangle = \sum_{j=0}^{m-1} e^{-i(E_m - E_0)\Delta t}|\Phi_j\rangle\langle\Phi_j|\Psi(t)\rangle + e^{-i(\hat{H}(t)-E_0)\Delta t}(1-\hat{P})|\Psi(t)\rangle, \tag{15}$$

in which the sparse matrix exponential is only operated on the subspace orthogonal to the m lowest eigenstates, and the ground-state energy E_0 is introduced to reduce the amplitude of the oscillations by making the diagonal elements of $\hat{H}$ smaller.

Besides using the eigenstates of the Hamiltonian as the basis for the expansion of $|\Psi(t)\rangle$, the operation of large matrix exponential has also been recently utilised through forming the Krylov subspace by successive Gram–Schmidt orthonormalisation of the set $\{|\Psi\rangle, -i\hat{H}\Delta t|\Psi\rangle, (-i\hat{H}\Delta t)^2|\Psi\rangle, \ldots\}$ [23], or expanding the time-evolution operator in Chebyshev polynomials [36].

Because the truncated Hilbert space in the static t-DMRG scheme of CM [18] is not updated during the time evolution, the critical factor for the validity of this approach is that the truncated space for the ground state of the $t = 0$ Hamiltonian $\hat{H}(t = 0)$ will be capable of representing the states that will be visited by the time-dependent Hamiltonian $\hat{H}(t)$ during time evolution [14]. However, this assumption breaks down in many applications [19]. In order to improve this situation, Luo, et al. [19] and Schmitteckert [21] suggested using $\hat{\rho} = \sum_{i=0}^{N_t} \alpha_i |\Psi(t_i)\rangle\langle\Psi(t_i)|$ (the weight factors α_i fulfilling $\Sigma\alpha_i$=1), a density matrix that is given by a superposition of states at different times of the evolution, is much more accurate. Even so, the deviation of $|\Psi(t)\rangle$ from $|\Psi(t = 0)\rangle$ increases with the evolving time, and accordingly more and more states are necessary to be kept in the truncated Hilbert space during time evolution. Such high demanding for the computational costs greatly prevents the static t-DMRG from long-time simulations.

While the approaches by Luo, et al. [19] and Schmitteckert [21] targeted the entire range of simulation time during the construction of RDMs of the subsystems, requiring more RDM eigenstates to be kept and slowing the calculation, Feiguin and White argued that targeting

only a small interval of time ($t \to t + \Delta t$) by

$$\hat{\rho} = \frac{1}{3}|\Psi(t)\rangle\langle\Psi(t)| + \frac{1}{6}|\Psi(t+\Delta t/3)\rangle\langle\Psi(t+\Delta t/3)| + \frac{1}{6}|\Psi(t+2\Delta t/3)\rangle\langle\Psi(t+2\Delta t/3)| + \frac{1}{3}|\Psi(t+\Delta t)\rangle\langle\Psi(t+\Delta t)| \quad (16)$$

can significantly improve the t-DMRG accuracy with an application in calculating the excitation spectrum of the Heisenberg ladder [22]. Such a scheme was also recently applied to compute the complex polarisation function in linear hydrogen chains with ab initio Hamiltonians by Ronca et al. [68] However, it was found that the state average scheme including wave functions at different time steps can be counterproductive in some cases. It is explained by the fact that $|\Psi(t)\rangle$ at the beginning of a time step, represented in the renormalised basis at time t, becomes approximated by the renormalised basis at time $t + \Delta t$ at the end of the time step, introducing an error in the representation of the initial state. Thus, Ronca et al. [68] suggested to use independent MPS to describe states at different times.

4. Adaptive time-dependent density matrix renormalisation group

4.1. Basic algorithm

In order to improve the accuracy for the operation of time-evolution operator and the representation of the time-evolving states within a truncated space, in 2004 Daley et al. [26] and White and Feiguin [25] proposed the adaptive t-DMRG method, which is an extension of standard DMRG using Vidal's TEBD algorithm [38]. Time evolution in the adaptive t-DMRG is generated using the Trotter-Suzuki decomposition of the time-evolution operator $U(\Delta t) = \exp(-i\hat{H}(t)\Delta t/\hbar)$. Assuming the Hamiltonian operator can be decomposed into a sum of local terms $\hat{h}_n$ that live only on neighbouring sites n and $n + 1$, i.e. $\hat{H} = \sum_{n=1}^{N} \hat{h}_n$, $U(\Delta t)$ can be approximated by an nth-order Trotter-Suzuki decomposition [40], e.g. to second order,

$$U(\Delta t) = \prod_{n\in\text{even}} U_n(\Delta t/2) \prod_{n\in\text{odd}} U_n(\Delta t) \prod_{n\in\text{even}} U_n(\Delta t/2) + O(\Delta t^3). \quad (17)$$

The $U_n(\Delta t)$ are the infinitesimal time-evolution operators $\exp(-i\hat{h}_n(t)\Delta t/\hbar)$ on 1D neighbouring sites n and $n + 1$. The ordering within the even or odd products does not matter, because 'even' and 'odd' operators commute among themselves. Then we can incorporate the implementations of these operators $U_n(\Delta t)$ successively to some state $|\psi\rangle$ into finite-system DMRG sweeps [1,14]. Each operator $U_n(\Delta t)$ is applied at a finite-system DMRG step with sites n and $n + 1$ being the active sites, i.e. where sites n and $n + 1$ are represented without truncation. For example, in a L-site 1D chain, by using the notions of MPS [59–61] and MPO [62,63], it is easy to describe the new state after the operation of $U_n(\Delta t)$ by

$$U_n(\Delta t)|\Psi\rangle = \sum_{\sigma_n'\sigma_{n+1}'} \sum_{\sigma_1\ldots\sigma_L} U_n(\Delta t)_{\sigma_n'\sigma_{n+1}',\sigma_n\sigma_{n+1}} A^1[\sigma_1]\ldots A^n[\sigma_n']A^{n+1}[\sigma_{n+1}']\ldots A^L[\sigma_L]|\sigma_1\ldots\sigma_n'\sigma_{n+1}'\ldots\sigma_L\rangle \quad (18)$$

without any additional error, because $U_n(\Delta t)$ only acts on the part of Hilbert space ($|\sigma_n\rangle|\sigma_{n+1}\rangle$) which is exactly represented. Similar to conventional DMRG, in order to prevent the exponential growth of matrix dimension for continuing the finite-system sweep, DMRG truncations must be carried out. But differently, the adaptive t-DMRG uses $U_n(\Delta t)|\Psi\rangle$ as the target state instead of $|\Psi\rangle$ to build the reduced density matrix. At the end of several sweeps, when all the local time-evolution operators have been applied successively to $\Psi(t)$, one can get the new wavefunction $\Psi(t + \Delta t)$ for the time $t + \Delta t$, and continue to longer times. In the context of 1D electronic and bosonic systems, the adaptive t-DMRG has been found to be a highly reliable method, for example in the context of spin-charge separation in cold Fermi gases [41], dynamical quasicondensation of hard-core Bosons at finite momenta [42], and far-from-equilibrium properties of interacting nanostructures [43], as well as many others [44–56].

4.2. Algorithm for electron-phonon systems

In reality, no quantum system is completely isolated from its surroundings, thus every quantum system is open to an environmental bath, which leads to dissipation. Environment-induced dissipation and coherence/decoherence play a crucial role in ultrafast optoelectronic processes in biological photosynthetic systems and organic semiconductors [57,69–73]. Therefore, the incorporation of the system-bath interaction into t-DMRG simulations becomes a necessity for systems embedded in a non-negligible environment.

A simple way to deal with dephasing and relaxation is to integrate Lindblad or Bloch-Redfield master equations based on the assumptions of weak system-bath coupling and the Markov approximation. For example, Cai and Barthel recently implemented the adaptive t-DMRG to evolve the Lindblad master equation to investigate the decoherence in spin-1/2 chains with uniform local

couplings to a Markovian environment [50]. However, the assumption that the correlation time of the environments is much faster than that of the system dynamics is frequently not justified in many realistic systems, and moreover, in the limit of slow bath dynamics, perturbative treatments of the system-bath coupling cannot be used even if this coupling is intrinsically weak [29].

Another economic solution is to use mixed quantum-classical dynamics, in which the whole system is separated into two parts: a fast varying, quantum mechanical part (for example, electrons (x)) and a slowly varying part (for the much heavier nuclei (y)) at the classical limit [74]. One of the popular approaches for mixed quantum-classical dynamics is Ehrenfest mean-field method, in which the classical part is under the force of a mean-field generated by the quantum part. The simplest propagation equation reads

$$\begin{aligned} i\hbar\frac{\partial}{\partial t}|\Psi(x,t)\rangle &= \hat{H}(x,y,t)|\Psi(x,t)\rangle, \\ \ddot{y}(t) &= \nabla_y V_E(y(t)), \end{aligned} \tag{19}$$

where the Ehrenfest mean-field potential is calculated by

$$V_E(y(t)) = \langle\Psi(x,t)|\hat{H}(x,y,t)|\Psi(x,t)\rangle. \tag{20}$$

It should be noted that the gradient of Ehrenfest mean-field potential $\nabla_y V_E(y(t))$ can be calculated analytically or numerically, depending on the formula of the Hamiltonian. For a Su–Schrieffer–Heeger–Hubbard model, H.M. [27] and Y.Y. [28] and their colleagues derived the analytical formula for the potential gradient, and then implemented real-time simulations by virtue of iteratively evolving the electronic wavefunction by the adaptive t-DMRG method and moving the nuclei by the classical mechanics. This t-DMRG-based Ehrenfest mean-field dynamics approach has been successfully applied to the study of the charge carrier dynamics in conjugated polymers under external fields [27,28,75–79].

Strong system-bath couplings require a full quantum treatment of both the system freedoms and the bath ones, but the system-bath Hamiltonian is usually not in the form of 1D chain with only nearest-neighbour hopping, which is a prerequisite for the adaptive t-DMRG simulation. In 2010, Chin et al. [80] proved that, by using the properties of orthogonal polynomials, it is possible to have an exact unitary transformation that maps the Hamiltonian of a quantum system coupled linearly to a continuum of bosonic or fermionic modes

$$\begin{aligned} \hat{H} &= \hat{H}_{\text{system}} + \hat{H}_{\text{bath}} + \hat{V}_{\text{s-b}} \\ &= \hat{H}_{\text{system}} + \int_0^{\nu\max} d\nu g(\nu) a_\nu^\dagger a_\nu \\ &\quad + \int_0^{\nu\max} d\nu h(\nu)\hat{A}(a_\nu^\dagger + a_\nu) \end{aligned} \tag{21}$$

to a Hamiltonian that describes a 1D chain with only nearest-neighbour interactions

$$\begin{aligned} \hat{H}' &= \hat{H}_{\text{system}} + c_0\hat{A}(b_0 + b_0^\dagger) \\ &\quad + \sum_{n=0}^{\infty}(\omega_n b_n^\dagger b_n + t_n b_{n+1}^\dagger b_n + t_n b_n^\dagger b_{n+1}), \end{aligned} \tag{22}$$

as schematized in Figure 2**.** This theory was then suggested to be combined with the adaptive t-DMRG algorithm for efficient simulation of strong system-bath interactions by Prior et al. [29]. Such an adaptive t-DMRG approach with a prerequisite mapping transformation for the Hamiltonian has been recently successfully applied to study the ultrafast electronic processes in organic condensed phase with a large number of vibrational modes [57,58].

5. Time-evolving MPS

Using the language of MPS and MPO, t-DMRG has also been re-formulated recently by Haegeman et al. [31,32] for studying time evolution based on TDVP [64,65]. Because the decomposition of the Hamiltonian into many local terms by TEBD is not required by such a formulation, it can be coped with arbitrary Hamiltonians, including those with long-range interactions and higher-dimensional problems with short-ranged interactions. Here we will briefly introduce the procedures in this formulation. If one uses the MPS representation of the DMRG wavefunction as in Equation (5) with the centre active site n, the time evolution can be obtained by only making $A_C(n)$ time-dependent and letting it satisfy $\dot{A}_C(n,t) = -i\hat{H}(n)A_C(n,t)$, where $\hat{H}(n)$ is the one-site effective Hamiltonian as defined in Figure 3. Thus, we can evolve $A_C(n)$ by

$$A_C(n,t) = e^{-i\hat{H}(n)t}A_C(n,0). \tag{23}$$

Similarly, the C matrix in Equation (8) can be evolved by

$$C(n,t) = e^{+i\hat{K}(n)t}C(n,0), \tag{24}$$

where $\hat{K}(n)$ is the zero-site effective Hamiltonian as defined in Figure 3. The evolution of C in Equation (24) can be interpreted as an evolution backwards in time. The detailed evolution of the total MPS from t to $t + \Delta t$ can be accomplished by stating with n=1 and repeating the following steps: Evolve $A_C(n, t)$ according to in Equation (23) for a time step δt. Factorise the updated

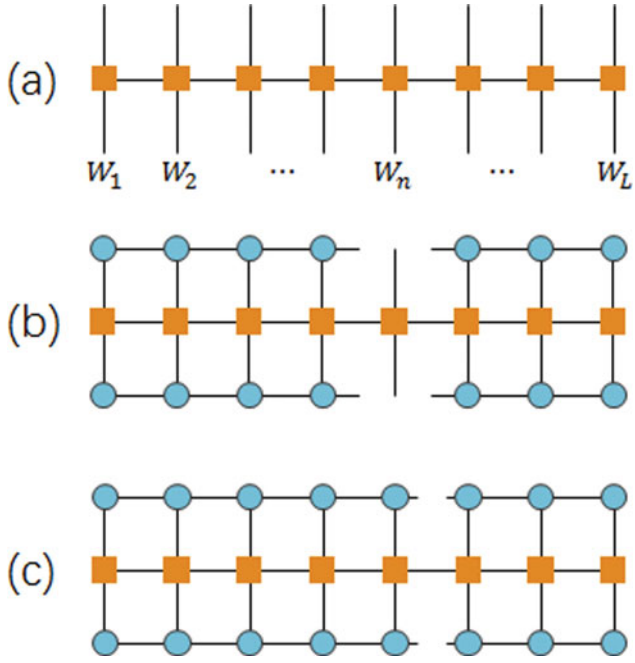

Figure 3. (a) Graphical representation of a matrix product operator (MPO) $\hat{H} = W^{\sigma_1'\sigma_1} W^{\sigma_2'\sigma_2} \ldots W^{\sigma_L'\sigma_L}$. (b) Graphical representation of a one-site effective Hamiltonian $\hat{H}(n)$. (c) Graphical representation of a zero-site effective Hamiltonian $\hat{K}(n)$, which can be easily computed from $\hat{H}(n)$.

$A_C(n, t + \Delta t) = A_L(n, t + \Delta t)C(n, t + \Delta t)$. Evolve $C(n, t + \Delta t)$ backwards in time according to Equation (24) and generate $A_C(n + 1, t) = C(n, t)A_R(n + 1, t)$. Usually one defines a half-sweep or a complete sweep (left and right) for updating all A matrices as a single time integration step for Δt.

Another effective method to study time evolution of long-range interacted systems in the context of MPS is using MPO. If a long-ranged Hamiltonian $\hat{H}$ has a compact MPO approximation for time evolution operator $\hat{U}(t) = e^{-it\hat{H}}$, then the time evolution can be efficiently simulated by successively applying the MPO to the MPS. In 2015, Zaletel *et al.* [33] proposed an approach to construct such time-evolving MPOs. In many cases, it is difficult to find a compact MPO approximation for $\hat{U}(t)$. But it is still possible to implement efficient real-time evolution of long-range interacted systems though Runge-Kutta numerical integration by applying $\hat{H}$ instead of $\hat{U}(t)$ to the wavefunction $\Psi(t)$ according to Equations (12) and (13), if one can find a compact MPO representation for $\hat{H}$.

6. Applications of t-DMRG on electron-phonon systems

Organic molecular systems are always associated with complicated vibrational spectrum (phonon structures). Electrons couple to the phonons via electrostatic interaction between the electron and nucleus, such that the exciton dynamics and charge transportation are heavily modulated by the phonons. In detail, the fast-vibration modes influence the quantum coherence of excitons and charges, and the slow-vibration modes serve as the origin of self-trapping effect which induces either spatially localised polarons or dynamic disorders depending on the electron-phonon coupling strength. The former should obviously be treated quantum-mechanically, while the latter is commonly simplified into classical phonons. Below we will briefly introduce three examples of our t-DMRG simulations for electron-phonon systems.

6.1. Dissociation of a triplet exciton in a polymer chain

Singlet fission, the quantum mechanical process by which a singlet exciton splits into two distinct triplet excitons, has recently attracted lots of research interests due to its proposed use for carrier multiplication in organic solar cells (OSCs) [81]. However, the dissociation mechanism of the triplet exciton is still quite few, in contrast to the intense study for the dissociation of singlet excitons. In this part, we show our t-DMRG numerical simulations for the triplet exciton dissociation in a polymer chain.

We model a donor/acceptor heterojunction interface structure with a 100-site 1D chain, composing of a 84-site conjugated polymer coupled with an 8-site 1D electron donor molecule at the left side and an 8-site 1D electron acceptor molecule at the right side. The 1D chain involving both electron and classical phonons could be described by a Su-Schrieffer-Heeger (SSH) model plus the extended Hubbard model [27,28,75–79]. The π-electron part includes both the electron-phonon and the electron–electron interactions,

$$\begin{aligned} H_e = & -\sum_{\langle n,n'\rangle,\sigma} t_{n,n'}(c^{\dagger}_{n',\sigma}c_{n,\sigma} + h.c.) \\ & + \frac{U}{2}\sum_{n,\sigma}\left(c^{\dagger}_{n,\sigma}c_{n,\sigma} - \frac{1}{2}\right)\left(c^{\dagger}_{n,-\sigma}c_{n,-\sigma} - \frac{1}{2}\right) \\ & + V\sum_{\langle n,n'\rangle,\sigma,\sigma'}\left(c^{+}_{n,\sigma}c_{n,\sigma} - \frac{1}{2}\right)\left(c^{\dagger}_{n',\sigma'}c_{n',\sigma'} - \frac{1}{2}\right) \\ & + \sum_{n,\sigma}\mu_n c^{\dagger}_{n,\sigma}c_{n,\sigma} \end{aligned} \tag{25}$$

where $t_{n,n'}$ is the hopping integral between the n-th site and the n'-th site, while U is the on-site Coulomb interaction and V denotes the nearest-neighbour electron–electron interaction. $\langle n, n'\rangle$ denotes the summation over nearest-neighbouring sites. μ_n is the on-site potential introduced to tune the electron affinity of the n-th site,

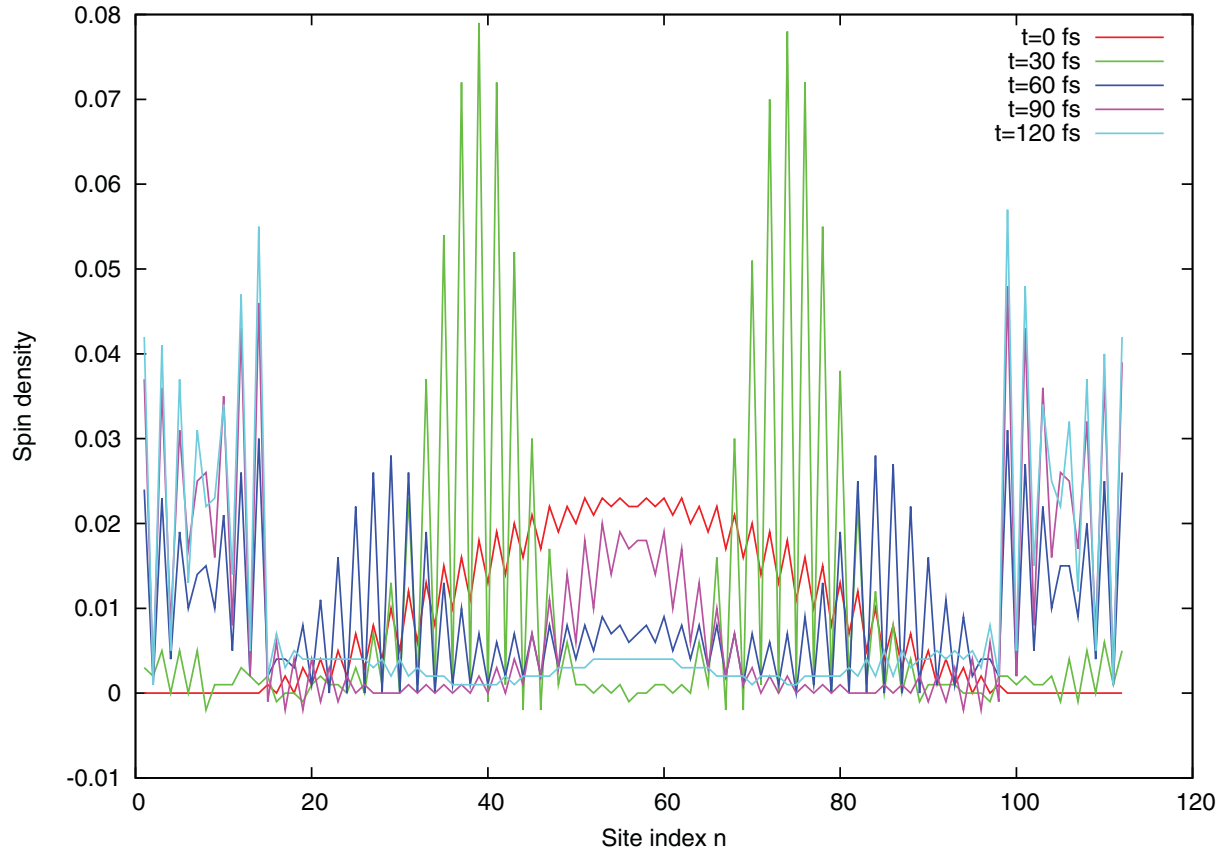

Figure 4. Time evolution of the spin density on the polymer chain.

therefore it is set as zero for the central polymer chain ($n = 9, 10, \ldots, 92$) and it will be positive for the left electron donor molecule and negative for the right electron acceptor molecule. The phonon Hamiltonian is described as

$$H_{\mathrm{p}} = \frac{K}{2}\sum_{j}(u_{j+1} - u_j)^2 + \frac{M}{2}\sum_{j}\dot{u}_j^2, \tag{26}$$

where K is the elastic constant originating from the σ-bonds between carbon atoms and M the mass of a site.

The dynamics of the system relies on the Schrödinger equation for the electrons and the Newtonian equation for the classical phonons. The key issue turns out to be the crossover between these two equations. One way on the mean-field level is the so-called Ehrenfest dynamics, in which the reduced density matrix of the electrons is utilised in the Newtonian equation. Namely, the temporal evolution of the phonons can be obtained by solving the following equation:

$$\begin{aligned} M\ddot{u}_j(t) = {} & K[u_{j+1}(t) + u_{j-1}(t) - 2u_j(t)] \\ & + 2\alpha\mathrm{Re}[\rho_{j,j-1}(t) - \rho_{j+1,j}(t)] - M\eta\dot{u}_j, \end{aligned} \tag{27}$$

where η is the damping coefficient and ρ is the reduced density matrix defined as

$$\rho = |\Psi(t)\rangle\langle\Psi(t)|, \tag{28}$$

with $\Psi(t)$ being the time-dependent wavefunction of electrons. If we intend to calculate the dynamics of a polaron, for example, $\Psi(t)$ is computed by t-DMRG with the total number of electron being $N + 1$ and N being the number of site on the lattice.

Herein, we take an example of triplet exciton dissociation as shown in Figure 4. In the computations, the model parameters are those generally chosen for polyacetylene: $t_0 = 2.5$ eV, $\alpha = 4.1$ eV/Å, $K = 21$ eV/Å^2, $M = 1349.14$ eVfs^2/Å^2, $a = 1.22$ Å. In order to consider the intermolecular hopping, we assume hoppings exist between the donor and acceptor molecules and the hopping integral in the centre of the chain is set as 0.5 eV. It is shown that upon photoexcitation the spin density wave is formed in the central part of the conjugated polymer. Due to the strong electron–phonon couplings within conjugated systems, there is strong connection between electronic structure and geometric structure. Therefore, the π-conjugated system tends to relax down to the bottom of the potential energy surface of the lowest triplet excited

state. As could be found in Figure 4 that two spin density peaks emerge and depart from each other gradually before they become close to the electron donor/acceptor part. This is a soliton–antisoliton picture for the lowest triplet excited state which has been revealed by previous theoretical studies [82]. We also notice that such soliton–antisoliton pair picture dissapears after the triplet exciton is diffused to the donor–acceptor interface and the spin density waves are then transferred to the electron donor and acceptor parts through electron hoppings. We do not find polaron-pair states during the charge separation process.

6.2. Singlet fission process in a molecular dimer

As we just introduced, the singlet fission is a process that a singlet exciton is split into two triplet excitons. In this subsection, we present our t-DMRG simulation of singlet fission in a dimer model in tetracene crystal. The model Hamiltonian is written as

$$H = H_{\mathrm{e}} + H_{\mathrm{p}} + H_{\mathrm{e-p}}. \tag{29}$$

Herein, the first term H_{e} represents the so-called Frenkel-charge transfer (CT) mixing model for the dimer [83], that is

$$H_{\mathrm{e}} = \sum_i |i\rangle E_i \langle i| + \sum_{i\neq j} |j\rangle V_{ij} \langle i|, \tag{30}$$

where $|i\rangle$ represents five possible states in the dimer, including two singlet states $|1\rangle \equiv |S_1, S_0\rangle$ and $|2\rangle \equiv |S_0, S_1\rangle$, two CT states $|3\rangle \equiv |C, A\rangle$ and $|4\rangle \equiv |A, C\rangle$ (C for cation and A for anion), and one TT state $|5\rangle \equiv |T_1, T_1\rangle$; E_i is the respective energy of the state, and V_{ij} is the transition energy from the state i to the state j. For the crystalline tetracene dimer, these parameters are taken from Parker et al.'s recent ab initio electronic structure calculation [84], in which the dimer wave function is constructed via an active space decomposition strategy using monomer wave functions computed by the restricted active space (RAS) method: $V_{13} = V_{31} = -0.051$ eV, $V_{14} = V_{41} = -0.074$ eV, $V_{23} = V_{32} = -0.118$ eV, $V_{24} = V_{42} = -0.111$ eV, $V_{35} = V_{53} = -0.081$ eV,$V_{45} = V_{54} = 0.056$ eV, and other V_{ij}'s are zero. We also set $E_{\mathrm{S1}}(\equiv E_1 = E_2) = 0.1$ eV, $E_{\mathrm{CT}}(\equiv E_3 = E_4) = 0.2$ eV, and $E_{\mathrm{TT}}(\equiv E_5) = -0.1$ eV.

The second and third term of Hamiltonian (29) read ($\hbar = 1$),

$$H_{\mathrm{p}} = \omega_{\mathrm{L}} \hat{a}^\dagger \hat{a} + \omega_{\mathrm{NL}} \hat{b}^\dagger \hat{b}, \tag{31}$$

$$H_{\mathrm{e-p}} = \gamma_{\mathrm{L}} |5\rangle\langle 5| (\hat{a}^\dagger + \hat{a}) + \gamma_{\mathrm{NL}} (|3\rangle\langle 3| + |4\rangle\langle 4|)(\hat{b}^\dagger + \hat{b}), \tag{32}$$

where $\hat{a}^\dagger(\hat{a})$ and $\hat{b}^\dagger(\hat{b})$ creates (annihilates) the local and nonlocal phonons with the frequency ω_{L} and ω_{NL}, and γ_{L} and γ_{NL} are the coupling, respectively. Herein, as we are concerning the dynamics of quantum coherence in the singlet fission process which is always of picosecond timescale, the phonons are treated quantum-mechanically. So far, it is not easy to determine the phonon modes that couples to the spin in an explicit manner, so we should take a continuous phonon spectrum instead. Without generality, we suppose that the phonon modes follow the similar spectral density function as that commonly utilised in the famous spin-boson model, namely, $J(\omega) = 2\pi\alpha\omega_c^{1-s}\omega^s e^{-\omega/\omega_c}$ with α being the dimensionless coupling strength, ω_c being the cutoff of the phonon frequency and s being the exponent. $s < 0.5$ denotes the regime of non-Markovian bath which would give rise to a long-standing quantum coherence.

In the perspective of t-DMRG, the quantum phonon bath cannot be straightforwardly dealt with except the bath is mapped to a lattice chain with the form being Equation (22). The mapping is actually available if we make use of the orthogonal-polynomials transformation to the bath, namely

$$\omega_\mu = \xi_s(P_\mu + Q_\mu), \tag{33}$$

$$t_\mu = -\xi_s P_\mu \left(\frac{N_{\mu+1}}{N_\mu}\right), \tag{34}$$

with

$$\xi_s = \frac{(s+1)[1-\Gamma^{-(s+2)}]}{(s+2)[1-\Gamma^{-(s+1)}]}\omega_c, \tag{35}$$

$$P_\mu = \frac{\Gamma^{-\mu}(1-\Gamma^{-(\mu+s+1)})^2}{[1-\Gamma^{-(2\mu+s+1)}][1-\Gamma^{-(2\mu+s+2)}]}, \tag{36}$$

$$Q_\mu = \frac{\Gamma^{-(\mu+s)}(1-\Gamma^{-\mu})^2}{[1-\Gamma^{-(2\mu+s)}][1-\Gamma^{-(2\mu+s+1)}]}, \tag{37}$$

$$N_\mu^2 = \frac{\Gamma^{-\mu(s+1)}(\Gamma^{-1};\Gamma^{-1})_\mu^2}{[\Gamma^{-(s+1)};\Gamma^{-1}]_\mu^2[1-\Gamma^{-(2\mu+s+1)}]}, \tag{38}$$

where

$$[a;q]_\mu = (1-a)(1-aq)\cdots(1-aq^{\mu-1}), \tag{39}$$

and Γ is the discretisation parameter. As shown in our papers [57,58], the orthogonal-polynomials representation for the quantum phonon bath is DMRG friendly and can lead to satisfactorily accurate results.

Figure 5 shows the time evolution of population on the states S_1S_0, S_0S_1, CA, AC and TT, respectively, with the initial state being S_1S_0. One can find there are two stages: In the first stage, the population on S_1S_0 quickly decreases and that on TT accordingly grows, which is explicitly the

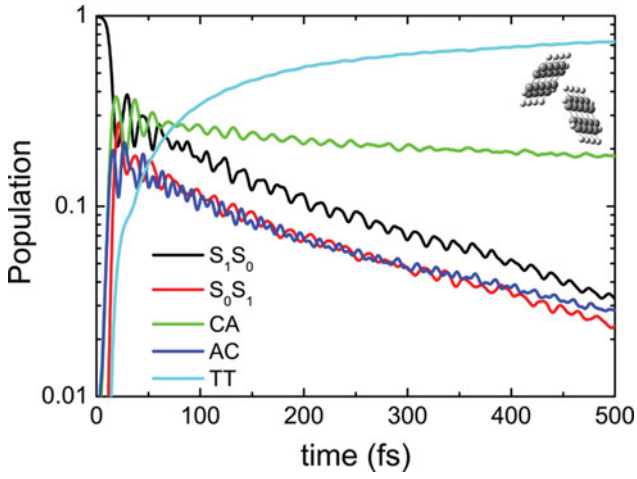

Figure 5. Time evolution of population on the states S_1S_0, S_0S_1, CA, AC and TT, respectively.

singlet fission process in an ultrafast timescale; In the second stage, the populations on these electronic states slowly change and importantly there emerges beating modes for both singlet and CT states. The beating stems from the Davydov splitting as well as the participation of quantum phonons. Essentially, in the dynamics we observe the change of CT population, which implies that the CT states do not just act as a virtual bridge state as some researchers stated. More discussions are referred to the relevant research article [57].

6.3. Intersystem crossing in pyrazine

t-DMRG could also be applied to simulate the nonadiabatic dynamics in realistic molecular or material system. Here, we take the intersystem crossing (IC) of a pyrazine molecule as an example. It is well known that there are two excited states S_1 and S_2 coupling to 24 vibrational modes [85–87]. The first state S_1 corresponds to the normal $\pi - \pi^*$ process, while the second state S_2 is a vibronic one with relatively broad absorption spectrum. The transition between these two states, namely the IC, has been clearly determined on the experimental side. It is thus a very good benchmarking instance for the dynamics approach to test computing the spectral features.

The Hamiltonian for describing the relaxation from S_2 to S_1 can be written as

$$H = H_e + H_p. \tag{40}$$

Herein, the first term H_e represents the Hamiltonian for the two excited states, namely

$$H_e = \begin{pmatrix} -\Delta & 0 \\ 0 & \Delta \end{pmatrix},$$

where Δ is the energy of the excited state. The phonon parts of the Hamiltonian writes

$$H_p = \sum_\nu \omega_\nu \hat{a}_\nu^\dagger \hat{a}_\nu + (\hat{a}_1^\dagger + \hat{a}_1) \cdot \begin{pmatrix} 0 & \lambda \\ \lambda & 0 \end{pmatrix} + \sum_{\nu \neq 1} (\hat{a}_\nu^\dagger + \hat{a}_\nu) \cdot \begin{pmatrix} \kappa_\nu^1 & 0 \\ 0 & \kappa_\nu^2 \end{pmatrix},$$

where the first vibrational mode off-diagonally couples to the excited states with the coupling strength being λ, and the other modes diagonally couple to the excited states with the coupling strength being κ^1 and κ^2, respectively. The frequency and coupling strength could be found in Ref. [85]. There are four primary modes out of the 24:

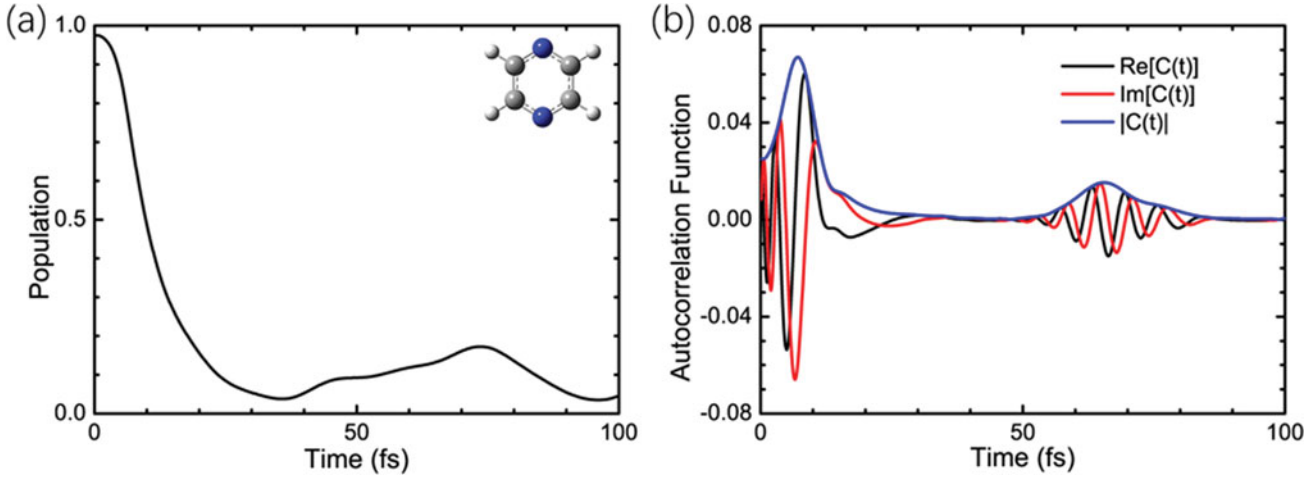

Figure 6. Time evolution of (a) population of S_2 and (b) autocorrelation function in a pyrazine molecule.

Three of them are diagonal coupling modes, and the remaining one is the off-diagonal mode.

Figure 6 shows the results of both population and autocorrelation function in pyrazine. As known from the experimental absorption spectrum, when the initial state is S_2, there will be an obvious recurrence at 60–80 fs. This most pronounced feature of pyrazine has been well captured by the t-DMRG simulation, as one can find in both population and autocorrelation function evolution a bulge at around 70 fs. The primary vibrational modes are responsible for this feature, implying that the t-DMRG has essentially got the proper phonon structure of the realistic molecule. However, we would also like to say that, the fine details of the dynamics are still not fully rebuilt since the off-diagonal coupling challenges almost all the quantum dynamics method. Through comparing with other numerical results, it is undoubtedly the t-DMRG method that is able to be applied for the realistic systems. The improvements of t-DMRG algorithm for more accurate simulation of the excited-state nonadiabatic dynamics in pyrazine are still in progress.

7. Conclusion and outlook

In more than two decades, DMRG has been shown to be very accurate and efficient for finding the true equilibrium or steady-state quantities of (quasi-)1D large and strongly correlated systems and applied successfully to many fields, from physics to chemistry. Compared to other methods, DMRG has got well-controlled precision with moderate computational cost, and more importantly, it exhibits ready portability in different usage environment. On the other hand, a more strict theoretical framework, the MPS representation, participates in optimising and developing the algorithm, making the family of DMRG-based approaches more efficient and powerful. As one have read in this review, the DMRG method has been involved in from static to dynamic scenarios since 2002. The many variants of static and adaptive t-DMRG as well as time-evolving MPS provide new means to explore the real-time quantum dynamics, including responses to the external time-dependent perturbations and their dynamics far from equilibrium. As reviewed, e.g. the t-DMRG approach has been recently applied to several realistic chemical problems such as the exciton dissociation in the polymer chain, the singlet fission in acenes and the IC in pyrazine. Nevertheless, while quantum chemistry theory brought DMRG into the framework in a very early stage, it is not completed yet. Two essential issues should still be carefully considered in t-DMRG: the long-range electronic coupling and the electron-phonon coupling.

In realistic molecular systems, electrons interact with each other via the long-range Coulomb force, so that the long-range interactions are essential in dealing with a realistic chemical system. DMRG, in a traditional manner, loses its precision of several orders while dealing with the long-range interaction. This is because the nonlocal correlation induced by the long-range interaction makes the reduced density matrix maximally mixed and a number of important states are thrown away during the DMRG truncation. Recent advances fixed this problem to an extent by considering many improvements, e.g. doubling the time window for targeting the wavefunction [24], or time-evolving a MPS by using compact MPOs [33]. Rather, one should still figure out the balance between the precision and efficiency before dealing with long-range interactions. Phonons are the other critical ingredient in mimicking the realistic systems, especially organic molecules. The basic difficulty of simulating phonon system stems from the infinite dimension of the local Fock space. So far, we have not got a generic and systematic way for this long-standing problem, since we can only deal with the systems with relatively weak electron-phonon coupling which induces very few phonons in each mode. In addition, when the off-diagonal couplings taken into account are with the strength comparable to those of diagonal couplings, the ground state will get high degeneracy and the method collapses very easily. In 2016, we have developed a method, so-called the symmetrically optimised phonon basis, which may serve as a settlement for this issue [88]. Moreover, for the relatively strong coupling cases, there are two possible ways to go. The first way is transforming the bare phonon states to coherent states in the local space. Based on this idea, one has to develop an approach to determine the effective displacement for each coherent state; The variational method might be in play. The second way is trying to separate the Fock space of one mode into several sites by either a direct division or an effective mapping based on some kind of symmetry. By doing so, the problem of phonons comes down to the problem of long-range interaction, and one can then adopt the methods that are efficient for the latter.

Compared with other full quantum dynamics approaches, such as the multi-configuration time-dependent Hartree (MCTDH) [89], quasi-adiabatic path integral (QUAPI) [90] and hierarchy equations of motion (HEOM) [91], t-DMRG is in some case easy to be adapted for different physical models. It consumes relatively short computing time for a certain degree of precision. Rather, the code of t-DMRG is somehow complicated for a new entrant. There are also a few issues that are still not solved. An example is the initial state for time evolution. In the framework of DMRG, an initial state must be obtained via complicated optimising

processes: It is not very convenient to construct a specific initial state of interest. In particular, when one intends to calculate the coherent electronic spectra, one has to calculate the time evolution of a series of initial states. In this context, the development of new approaches for constructing a certain initial state is still in demand.

Once we are on the stage of efficient time evolution computation, it is quite rational to move on to the spectral simulations through the Fourier transformation from the time domain to the frequency domain. So far, main investigations focus on the cold atoms and strongly-correlated systems. For instance, the one-dimensional Hubbard model as well as the Luttinger liquid have been extensively studied, especially their photoemission spectra [92–94]. In these studies, the interaction is set to be rather strong so that the system is fully gapped and the t-DMRG approach could be pretty credible. For a generic model, the computation of Green function, which is the kernel of the spectra, suffers poor precision and efficiency.

Last but not the least, let us discuss more on the temperature effect. The state-of-the-art t-DMRG method works at zero temperature: there are very few researches on the development of finite-temperature DMRG or imaginary-time dependent DMRG. A rational strategy is to work in the Krylov representation to get the finite-temperature effect [21], but the efficiency is inadequate. Afterward, in order to run an efficient imaginary-time evolution of the states, there emerge several advanced methods. The first is the so-called minimally entangled typical quantum states developed by White, which comprises iterative measurements on the maximally entangled states to obtain the classical product states [95]. This method introduces stochastic operations making the precision poorly controlled. The second is to employ the Lanczos procedure to construct a reduced space for the excited states and thus calculate the evolution based on it [96]. The efficiency of this method depends on whether the Lanczos procedure produces sufficient set of typical states in the thermal equilibrium. The third is to additionally introduce auxiliary degrees of freedom which are maximally entangled with the system [97]. By tracing out the auxiliary ones, which consumes relatively large computing resources, the finite-temperature effect is subsequently obtained. To summarise, these finite-temperature DMRG methods have got their own drawbacks in practical applications, and thus it is meaningful in any ways to optimise and develop the algorithm.

Disclosure statement

No potential conflict of interest was reported by the authors.

Funding

National Natural Science Foundation of China [grant number 21373109], [grant number 21673109], [grant number 21722302], [grant number 91333202] and [grant number 11574052].

References

[1] S.R. White, Phys. Rev. Lett. **69**, 2863 (1992).
[2] S. Yan, D.A. Huse, and S.R. White, Science **332**, 1173 (2011).
[3] S.D. Geraedts, M.P. Zaletel, R.S.K. Mong, M.A. Metlitski, A. Vishwanath, and O.I. Motrunich, Science **352**, 197 (2016).
[4] R.D. Somma, C.D. Batista, and G. Ortiz, Phys. Rev. Lett. **99**, 030603 (2007).
[5] Z. Shuai, S.K. Pati, J.L. Brédas, and S. Ramasesha, Synthetic Met. **85**, 1011 (1997).
[6] S. Ramasesha, S.K. Pati, H.R. Krishnamurthy, Z. Shuai, and J.L. Brédas, Synthetic Met. **85**, 1019 (1997).
[7] G.K.-L. Chan and S. Sharma, Annu. Rev. Phys. Chem. **62**, 465 (2011).
[8] Y. Kurashige, G.K.-L. Chan, and T. Yanai, Nat. Chem. **9**, 660 (2013).
[9] S. Sharma, K. Sivalingam, F. Neese, and G.K.-L. Chan, Nat. Chem. **6**, 927 (2014).
[10] S. Wouters and D. Van Neck, Eur. Phys. J. D **68**, 272 (2014).
[11] S. Szalay, M. Pfeffer, V. Murg, G. Barcza, F. Verstraete, R. Schneider, and Ö. Legeza, Int. J. Quant. Chem. **115**, 1342 (2015).
[12] Ö. Legeza and J. Sólyom, Phys. Rev. B **70**, 205118 (2004).
[13] C. Duperrouzel, P. Tecmer, K. Boguslawski, G. Barcza, Ö. Legeza, and P.W. Ayers, Chem. Phys. Lett. **621**, 160 (2015).
[14] U. Schollwöck, Rev. Mod. Phys. **77**, 259 (2005).
[15] K. Hallberg, J. Comput. Theor. Nanosci. **5**, 1 (2008).
[16] U. Schollwöck, Ann. Phys. **326**, 96 (2011).
[17] U. Schollwöck, Phil. Trans. R. Soc. A **369**, 2643 (2011).
[18] M.A. Cazalilla and J.B. Marston, Phys. Rev. Lett. **88**, 256403 (2002).
[19] H.G. Luo, T. Xiang, and X.Q. Wang, Phys. Rev. Lett. **91**, 049701 (2003).
[20] M.A. Cazalilla and J.B. Marston, Phys. Rev. Lett. **91**, 049702 (2003).
[21] P. Schmitteckert, Phys. Rev. B **70**, 121302 (2004).
[22] A. Feiguin and S.R. White, Phys. Rev. B **72**, 020404 (2005).
[23] U. Schollwöck, J. Phys. Soc. Jpn. **74**, 246 (2005).
[24] T. Dutta and S. Ramasesha, Phys. Rev. B **82**, 035115 (2010).
[25] S.R. White and A. Feiguin, Phys. Rev. Lett. **93**, 076401 (2004).
[26] A.J. Daley, C. Kollath, U. Schollwöck, and G. Vidal, J. Stat. Mech. Theor. Exp. (2004), P04005.
[27] H. Ma and U. Schollwöck, J. Chem. Phys. **129**, 244705 (2008).
[28] H. Zhao, Y. Yao, Z. An, and C.Q. Wu, Phys. Rev. B **78**, 035209 (2008).

[29] J. Prior, A.W. Chin, S.F. Huelga, M.B. Plenio, Phys. Rev. Lett. **105**, 050404 (2010).
[30] F. Güttge, F.B. Anders, U. Schollwöck, E. Eidelstein, and A. Schiller, Phys. Rev. B **87**, 115115 (2013).
[31] J. Haegeman, J.I. Cirac, T.J. Osborne, I. Pizorn, H. Verschelde, and F. Verstraete, Phys. Rev. Lett. **107**, 070601 (2011).
[32] J. Haegeman, C. Lubich, I. Oseledets, B. Vandereycken, and F. Verstraete, Phys. Rev. B **94**, 165116 (2016).
[33] M.P. Zaletel, R.S.K. Mong, C. Karrasch, J.E. Moore, and F. Pollmann, Phys. Rev. B **91**, 165112 (2015).
[34] F.A.Y.N. Schröder and A.W. Chin, Phys. Rev. B **93**, 075105 (2016).
[35] D.M. Kennes and C. Karrasch, Comput. Phys. Commun. **200**, 37 (2016).
[36] J.C. Halimeh, F. Kolley, and I.P. McCulloch, Phys. Rev. B **92**, 115130 (2015).
[37] G. Vidal, Phys. Rev. Lett. **91**, 147902 (2003).
[38] G. Vidal, Phys. Rev. Lett. **93**, 040502 (2004).
[39] H.F. Trotter, Proc. Am. Math. Soc. **10**, 545 (1959).
[40] M. Suzuki, Commun. Math. Phys. **51**, 183 (1976).
[41] C. Kollath, U. Schollwöck, and W. Zwerger, Phys. Rev. Lett. **95**, 176401 (2005).
[42] L. Vidmar, J.P. Ronzheimer, M. Schreiber, S. Braun, S.S. Hodgman, S. Langer, F. Heidrich-Meisner, I. Bloch, and U. Schneider, Phys. Rev. Lett. **115**, 175301 (2015).
[43] E. Boulat, H. Saleur, and P. Schmitteckert, Phys. Rev. Lett. **101**, 140601 (2008).
[44] J. Sirker, R.G. Pereira, and I. Affleck, Phys. Rev. Lett. **103**, 216602 (2009).
[45] S.R. Manmana, S. Wessel, R.M. Noack, and A. Muramatsu, Phys. Rev. Lett. **98**, 210405 (2007).
[46] A.J. Daley, J.M. Taylor, S. Diehl, M. Baranov, and P. Zoller, Phys. Rev. Lett. **102**, 040402 (2009).
[47] C. Kollath, A. Iucci, T. Giamarchi, W. Hofstetter, and U. Schollwöck, Phys. Rev. Lett. **97**, 050402 (2006).
[48] T. Oka and H. Aoki, Phys. Rev. Lett. **95**, 137601 (2005).
[49] R.G. Pereira, S.R. White, and I. Affleck, Phys. Rev. Lett. **100**, 027206 (2008).
[50] Z. Cai and T. Barthel, Phys. Rev. Lett. **111**, 150403 (2013).
[51] K.R.A. Hazzard, S.R. Manmana, M. Foss-Feig, and A.M. Rey, Phys. Rev. Lett. **110**, 075301 (2013).
[52] S. Peotta, D. Rossini, M. Polini, F. Minardi, and R. Fazio, Phys. Rev. Lett. **110**, 015302 (2013).
[53] A. Feiguin, P. Fendley, M.P.A. Fisher, and C. Nayak, Phys. Rev. Lett. **101**, 236801 (2008).
[54] A.J. Daley, P. Zoller, and B. Trauzettel, Phys. Rev. Lett. **100**, 110404 (2008).
[55] J.-S. Bernier, R. Citro, C. Kollath, and E. Orignac, Phys. Rev. Lett. **112**, 065301 (2014).
[56] A. Rahmani, C.-Y. Hou, A. Feiguin, C. Chamon, and I. Affleck, Phys. Rev. Lett. **105**, 226803 (2010).
[57] Y. Yao, Phys. Rev. B **93**, 115426 (2016).
[58] Y. Yao, X. Xie, and H. Ma, J. Phys. Chem. Lett. **7**, 4830 (2016).
[59] M. Fannes, B. Nachtergaele, and R.W. Werner, Commun. Math. Phys. **144**, 443 (1992).
[60] S. Östlund and S. Rommer, Phys. Rev. Lett. **75**, 3537 (1995).
[61] S. Rommer and S. Östlund, Phys. Rev. B **55**, 2164 (1997).
[62] I.P. McCulloch, J. Stat. Mech. (2007) P10014.
[63] B. Pirvu, V. Murg, J.I. Cirac, and F. Verstraete, New J. Phys. **12**, 025012 (2010).
[64] P.A.M. Dirac, Proc. Cambridge Philos. Soc. **26**, 376 (1930).
[65] P.W. Langhoff, S.T. Epstein, and M. Karplus, Rev. Mod. Phys. **44**, 602 (1972).
[66] Ö. Legeza, J. Röder, and B.A. Hess, Phys. Rev. B **67**, 125114 (2003).
[67] Y. Saad, SIAM (Soc. Ind. Appl. Math.) J. Numer. Anal. **29**, 130 (1998).
[68] E. Ronca, Z. Li, C.A. Jimenez-Hoyos, and G.K.-L. Chan, J. Chem. Theory Comput. **13**, 5560 (2017). (doi:10.1021/acs.jctc.7b00682).
[69] G.D. Scholes, G.R. Fleming, L.X. Chen, A. Aspuru-Guzik, A. Buchleitner, D.F. Coker, G.S. Engel, R. van Grondelle, A. Ishizaki, D.M. Jonas, J.S. Lundeen, J.K. McCusker, S. Mukamel, J.P. Ogilvie, A. Olaya-Castro, M.A. Ratner, F.C. Spano, K.B. Whaley, and X. Zhu, Nature **543**, 647 (2017).
[70] J. Lim, D. Palecek, F. Caycedo-Soler, C.N. Lincoln, J. Prior, H. von Berlepsch, S.F. Huelga, M.B. Plenio, D. Zigmantas, and J. Hauer, Nat. Commun. **6**, 7755 (2015).
[71] Y. Song, S.N. Clafton, R.D. Pensack, T.W. Kee, and G.D. Scholes, Nat. Commun. **5**, 4933 (2014).
[72] E.J. O'Reilly and A. Olaya-Castro, Nat. Commun. **5**, 3012 (2014).
[73] A.W. Chin, J. Prior, R. Rosenbach, F. Caycedo-Soler, S.F. Huelga and M.B. Plenio, Nat. Phys. **9**, 113 (2013).
[74] J.C. Tully, Faraday Discuss. **110**, 407 (1998).
[75] H. Ma and U. Schollwöck, J. Phys. Chem. A **113**, 1360 (2009).
[76] H. Ma and U. Schollwöck, J. Phys. Chem. A **114**, 5439 (2010).
[77] H. Zhao, Y.G. Chen, X.M. Zhang, Z. An, and C.Q. Wu, J. Chem. Phys. **130**, 234908 (2009).
[78] H. Zhao, Y. Yao, Y.G. Chen, C.Q. Wu, X.M. Zhang, and Z. An, J. Chem. Phys. **131**, 154901 (2009).
[79] H. Zhao, Y.G. Chen, Y.H. Yan, Z. An, and C.Q. Wu, EPL **100**, 57005 (2012).
[80] A.W. Chin, A. Rivas, S.F. Huelga, and M.B. Plenio, J. Math. Phys. **51**, 092109 (2010).
[81] J. Xia, S.N. Sanders, W. Cheng, J.Z. Low, J. Liu, L.M. Campos, and T. Sun, Adv. Mater. **29**, 1601652 (2017).
[82] H. Ma, C. Liu, and Y. Jiang, J. Chem. Phys. **120**, 9316 (2004).
[83] T.C. Berkelbach, M.S. Hybertsen, and D.R. Reichman, J. Chem. Phys. **138**, 114103 (2013).
[84] S.M. Parker, T. Seideman, M.A. Ratner, and T. Shiozaki, J. Phys. Chem. C **118**, 12700 (2014).
[85] G.A. Worth, H.-D. Meyer, and L.S. Cederbaum, J. Chem. Phys. **105**, 4412 (1996).
[86] A. Raab, G.A. Worth, H.-D. Meyer, and L.S. Cederbaum, J. Chem. Phys. **110**, 936 (1999).
[87] M.A.C. Saller and S. Habershon, J. Chem. Theory Comput. **11**, 8 (2015).
[88] Y. Yao, N. Zhou, J. Prior, and Yang Zhao, Sci. Rep. **5**, 14555 (2015).
[89] M.H. Beck, A. Jackle, G.A. Worth, and H.D. Meyer, Phys. Rep. **324**, 1 (2000).
[90] N. Makri and D.E. Makarov, J. Chem. Phys. **102**, 4600 (1995).
[91] Y. Tanimura and R. Kubo, J. Phys. Soc. Jpn. **58**, 101 (1989).

[92] C. Kollath, A. Iucci, I.P. McCulloch, and T. Giamarchi, Phys. Rev. A **74**, 041604(R) (2006).
[93] A.E. Feiguin and D.A. Huse, Phys. Rev. B **79**, 100507(R) (2009).
[94] A.E. Feiguin and G.A. Fiete, Phys. Rev. B **81**, 075108 (2010).
[95] S.R. White, Phys. Rev. Lett. **102**, 190601 (2009).
[96] J. Kokalj and P. Prelovšek, Phys. Rev. B **80**, 205117 (2010).
[97] C. Karrasch, J.H. Bardarson, and J.E. Moore, Phys. Rev. Lett. **108**, 227206 (2012).